Cable route optimization for offshore wind farms in morphodynamic areas

Roetert, Tom; Raaijmakers, Tim; Borsje, Bas W.

Publication date
2017

Document Version
Final published version

Published in
Proceedings of the 27th International Ocean and Polar Engineering Conference, ISOPE 2017

Citation (APA)
Roetert, T., Raaijmakers, T., & Borsje, B. W. (2017). Cable route optimization for offshore wind farms in morphodynamic areas. In *Proceedings of the 27th International Ocean and Polar Engineering Conference, ISOPE 2017* (pp. 595-606). Society of Petroleum Engineers.

Cable route optimization for offshore wind farms in morphodynamic areas

Tom Roetert[1], Tim Raaijmakers[1,2], Bas Borsje[1,3]
[1] Deltares, unit Hydraulic Engineering, Delft, The Netherlands
[2] Technical University Delft, Offshore Engineering, Faculty of Civil Engineering, Delft, The Netherlands
[3] University of Twente, chair group Water Engineering and Management, Enschede, The Netherlands

ABSTRACT

The aim of this paper is to optimize power cable routing in a wind farm based on the expected morphological behaviour in the design lifetime of an offshore wind farm. Up to now methods to optimize cable route layout in offshore wind farms are only based on a flat seabed and do not take the seabed dynamics into account. For offshore wind farms, migrating seabed features in the form of sand waves are of great importance and may significantly alter the position of the seabed over the life time of the wind farm. This paper discusses the optimization of power cable routing in a morphodynamic seabed by assessing the power cable burial depth in both the vertical plane, e.g. buried deeper in areas where future seabed lowering is expected, and in the horizontal plane, e.g. diverting the power cables around risk prone areas. Outcomes of the proposed method showed both cost and risk reductions for the Hollandse Kust (zuid) Wind Farm case study compared to state-of-the-art optimization based on a fixed burial depth.

KEY WORDS: Power cables; route optimization; offshore wind; seabed morphodynamics; renewable energy; cost and risk reduction.

1 INTRODUCTION

Offshore wind farms are of great interest as renewable energy source. Over the years the demand for offshore wind energy rose due to scarcity of land, higher efficiency per wind turbine and an increasing energy demand. .

Figure 1: Designated wind farm areas in the Dutch North Sea. Note that the depicted MW's are changed (Netherlands Enterprise Agency, 2015)

In 2014, the Dutch government designated several areas in the North Sea for offshore wind farm development, as shown in figure 1. The wind farms in the Dutch North Sea should have a planned total capacity of 4,450 Megawatt in 2023, which is an enormous increase over today's 957 Megawatt offshore wind production.

Aimed at cost reduction in design, development and operation of offshore wind farms, a consortium of companies and knowledge institutions started the FLOW (Far and Large Offshore Wind) program. Part of this program was to investigate the optimization of the infield power cable layout.

1.1 Present cable optimization methods

Large parts of the sandy seabed of shallow seas, such as the North Sea, are covered with rhythmic bedforms, such as sand banks, sand waves and (mega) ripples. These features are dynamic and are the result of the complex interaction between hydrodynamics, sediment transport and morphology. Typical parameters of geometry and dynamics that distinguish different types of bedforms (wavelength, wave height and mobility) are presented in Figure 2. In the last column, the potential threat to foundations and electricity cables is indicated per bedform.

	Wavelength	Wave height	Mobility	Threat to foundations and cables
Ripples	O(0.1) m	O(0.01) m	Mobile and transient	Minimal
Megaripples	O(10) m	O(0.1) m	Mobile and transient	Minimal
Sand waves	**O(100) m**	**O(1) m**	**Mobile and persistent**	**Large**
Sand banks	O(1000) m	O(10) m	Stationary	Minimal

Figure 2: Morphodynamic seabed features and some typical characteristics. Capital "O(.)" indicates "In the order of" (Deltares, 2016).

For offshore wind farms, sediment transport in the form of sand waves is of great importance. These sand wave patterns can reach several meters in height, hundreds of meters in length and migration rates up to ten meter per year. Since large portions of the North Seabed are covered with these dynamic bedforms (Bijker et al., 1998; Borsje et al., 2013; Huntley et al., 1993), they should not be neglected in cable

routing. The dynamic character of sand waves is important for the integrity of power cables and may cause cable failure (Besio et al., 2004; Morelissen et al., 2003; Németh et al., 2002). As the sand waves migrate, a cable located near the sand wave crest may experience significant seabed lowering, which may make the cable vulnerable to anchors, fishnets or other threats. On the other hand, if a sand wave crest passes the cable that was formerly in a sand wave trough it may experience a significant increase in the burial depth, which locally may cause temperature increases around and thermal stresses inside the cable. Depending of the specifications of the cable and environmental requirements, this may be a problem.

Cables crossing a sand wave field, which spatially migrate with different speeds, may experience a local stress build-up due to an uneven strain. When combined with e.g. thermal stresses this may become critical. It is well known that cables exposed on the seafloor may experience local scour, which in some cases may be sufficient to undermine the cable, causing a free span. When combined with sand wave migration the risk of free spanning increases. A free span of a cable may, besides a local stress build up, also experience vortex induced vibrations. An example of sand waves influencing the burial depth is showed in Figure 3, depicting the interaction between pipelines and sand waves.

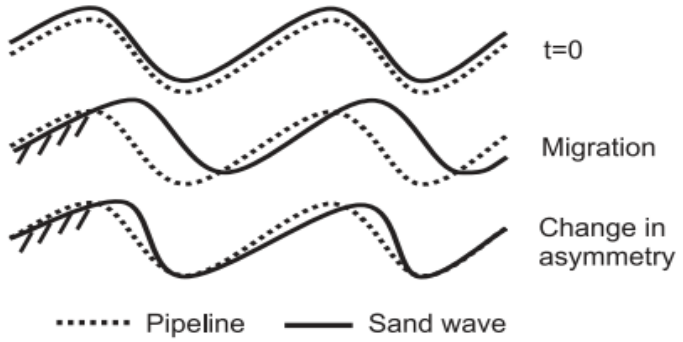

Figure 3: Effect of migrating sand waves on the burial depth of pipelines (Morelissen et al., 2003).

Because the cables still need to connect the wind turbines, the problem is also valid in the horizontal plane. A certain cable connection between two wind turbines may cross a sand wave field. The increased risk of failure can be overcome by diverting the cables around the sand wave field. However, the increased cable length implies extra costs. Therefore, in addition to the cable bending radius and the burial depth, the diversion is only accepted within a certain range (Németh, 2003).

Unfortunately, the current methods to optimize cable route design are not based on a dynamic seabed (Morelissen et al., 2003). Instead, route optimization is mainly based on algorithms describing a fixed wind farm layout(e.g. Jenkins et al., 2013), or a fixed wind farm layout containing fixed routing constraints described by Pillai et al. (2015), i.e. not accounting for dynamic constraints such as bed level changes. In addition, possible innovations in the cables are not investigated thoroughly. The result is that the design lifetime of power cables is not guaranteed. Up to now, cable optimization is mainly executed based on shortest routes given some constraints, instead of cost and risk reduction based on seabed dynamics.

Cable failure as a result of exposure is one of the highest risks in power cable installation. Within the offshore wind industry about 40 % of the number of insurance claims is related to failures of cables. Due to the high associated costs of a cable failure (lost energy revenues and high repair costs), the insurance costs for cable-related claims even amount up to 70-80 % of the total costs (Maurer, 2016). On average in Europe one export cable and about 10 inter-array cables fail every year. Roughly 1 in every 40 inter array cables fails during the lifetime of the wind farm (Maurer, 2016). Cable failures pose one of the highest risks as it can blackout an entire wind farm. In addition, cable monitoring and repair require expensive marine operations.

The aim of this paper is therefore to reduce risks of cable failure, by including sand waves and their dynamics in present methods to optimize cable layout As methods to develop a fixed wind farm layout are widely available, this paper mainly focusses on optimization of power cable routing based on the expected morphological behaviour in the design lifetime of an offshore wind farm. It was shown in Roetert (2014) that the static bed optimization under mild sloping bedforms (sand waves) does not increase cable length by much. Therefore it is decided to not include the results of this optimization step. Results should lead to a cost and risk reduction in cable installation and maintenance. To illustrate the results the Dutch offshore wind farm Hollandse Kust (zuid), that is still to be developed, is used as a case study.

The remainder of this paper is organized as follows. First in Section 2 the methods, functions and algorithms underlying the route optimization tools are described. Section 3 describes the steps taken to during the optimization steps, which are applied to a wind farm case study in a morphodynamic active environment in Section 4. Finally conclusions are drawn in Section 5.

2 ROUTE OPTIMIZATION

To combine present cable optimization methods with seabed dynamics we follow two steps: optimization under a flat bed and under a dynamic bed. The latter is split in optimization in the vertical plane and optimization in the horizontal plane. In this section all optimization algorithms and functions underlying the optimization steps are discussed. It must be stressed that route optimization based on wind yield of the turbines and in extension varying turbine power output is not taken into account in this research as the focus is on the interaction between seabed morphodynamics and cable burial depth.

2.1 Optimization under a flat seabed

In a wind farm located far offshore, the turbines are often connected to one or more offshore high voltage stations (OHVS) via cable strings. For costs savings, the aim is to minimize total weight of all cable connections, which is calculated from total cable length including extra weight from routing constraints. This problem can be seen as a combinatorial problem in which the costs of the total solution (total weight of all cable connections) of a finite set of objects (turbine connections) needs to be minimized. During this optimization step, the seabed is considered flat, such that seabed dynamics are not taken into account.

2.1.1 Combinatorial problem

In the real world many situations exist where a set of points need to be connected (Bondy & Murty, 1976). For example, the points can represent people and the connecting lines friendships. Also, a combination of cities and roads is possible. These connections can be modelled with the help of a graph.

A graph can be seen as an ordered triple G = $(V(G), E(G), \psi_G)$. The graph G exists of a nonempty set of nodes or vertices V(G) together with a set of lines or edges E(G) disjoint from V and a function ψ_G. Each vertex is indicated by a point and each edge by a line joining the

points. The points then will represent the ends of the lines. The function ψ_G associates each edge of G with a pair of vertices of G (Bondy & Murty, 1976). If e is an edge and u and v are vertices such that $\psi_G(e) = uv$, then edge e is said to join the vertices u and v. Figure 4 depicts and the formulas below provide an example given by Bondy and Murty (1976).

$$G = (V(G), E(G).\psi_G)$$

Where
$V(G) = \{v_1, v_2, v_3, v_4, v_5\}$
$E(G) = \{e_1, e_2, e_3, e_4, e_5, e_6, e_7, e_8\}$

In here ψ_G is defined by

$$\psi_G(e_1) = v_1v_2, \quad \psi_G(e_2) = v_2v_3,$$
$$\psi_G(e_3) = v_3v_3, \quad \psi_G(e_4) = v_3v_4,$$
$$\psi_G(e_5) = v_2v_4 \quad , \quad \psi_G(e_6) = v_4v_5,$$
$$\psi_G(e_7) = v_2v_5 \quad , \quad \psi_G(e_8) = v_2v_5$$

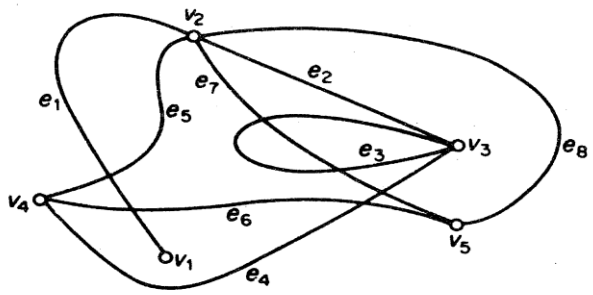

Figure 4: Diagram of graph described in example 1 (Bondy & Murty, 1976).

Wind farms can be seen as a graph with vertices, edges and one main point with every vertex connected to it. Where the wind turbines are the vertices, the power cables form the edges of the graph. Inside the layout, different solutions are possible to connect the nodes. For wind farms however, these solutions are limited (Jenkins et al., 2013). Bauer and Lysgaard (2015) refer the wind farm power cable layout problem as: find a set of open vehicle routes (strings) minimizing the total route costs, connecting every client (vertex) to a depot, not exceeding vehicle capacity (maximum numbers of vertices per string) and such that routes do not cross each other.

The optimization routine of the wind farm cable layout is both length , constraint-based and in extension thereof cost based. This means that every edge of the graph is given a certain weight, calculated from the length of each connection with addition of possible constraints along that specific connection. Possible constraints considered are: site boundaries, unexploded ordnances (UXO's), other cable corridors, unfavourable geological characteristics or areas with significant seabed level changes (order of >3 m, both upward and downward).Each constraint is judged on severity and a corresponding weight is added on top of the connection lengths. By judging or optimizing the severity, the option to route the cable around small constraints (e.g. UXO's) is left open and crossings of constraints covering larger areas (e.g. cable corridors) is minimized.

The problem implies that with aid of the weights of each connection an optimized route needs to be found, connecting every turbine to the OHVS with minimized total costs.

2.1.2 Genetic optimization algorithm

For solving the combinatorial problem, many solutions are proposed. These solutions vary from the exact methods, i.e. assessing all solutions to find the most optimal layout, to the classic heuristics and the meta-heuristics (Kumar & Panneerselvam, 2012). For the size and amount of solutions present in offshore wind farms, the genetic algorithm is found to be the most applicable.

The genetic algorithm applies the principles of evolution and adaptation to the environment that are present in every species to optimization problems. The application of the evolution principles finally leads to survival of the fittest (Caldeira, 2009). The genetic algorithm used is presented in Figure 5 and starts with the creation of an initial population. This initial population consists of multiple solutions for the layout problem. Each solution consists of one string containing all turbines in a random order, denoting turbine connectivity, with breaks indicating string ends. The amount of solutions is calculated form the number of turbines present, for example a set of 40 turbines has an initial population of 800 solutions. For each solution, the total weight is calculated by adding up all edges present in the solution. The weight of each edge is defined in a distance matrix containing all possible connections between either two turbines or a turbine and the OHVS. A solution consists of one string.

In the second step, the total population is divided in sets of eight solutions. The subset size is directly related to the number of mathematical operators introduced. Having both a sufficiently large population and a division in subsets diminishes risks of local optima being considered optimal as each subset is treated independently. Next the fitness of all solutions is evaluated, by assessing if all turbines are connected to the OHVS and if string capacity is not exceeded. The solution with the lowest total weight is then chosen as best solution in this set. The fourth step consists of applying eight mathematical operations independently to the best solution in a subset.

To illustrate the operators, each of the operators is applied to a conceptual wind farm consisting of ten turbines. The initial solution is described by the following string: [4 5 3 | 6 9 10 | 1 2 8]. Here the vertical lines denote string ends, resulting in a wind farm with three strings, each starting at the OHVS. Below each of the operators is described and applied to the initial solution of the conceptual wind farm. In the examples, the highlighted parts show adjustments made to the initial solution. To begin, during every iteration two random turbines (I and J) from the solution are chosen.

1. Flip the solution between turbine I and J;
   [4 5 3 7| 6 9 10| 1 2 8] → [4 5 9 6| 7 3 10| 1 2 8]
2. Swap turbine I and J in the solution;
   [4 5 3 7| 6 9 10| 1 2 8] → [4 5 9 7| 6 3 10| 1 2 8]
3. Slide the string between turbines I and J;
   [4 5 3 7| 6 9 10| 1 2 8] → [4 5 10 1| 3 7 6| 9 2 8]
4. Put turbine I directly behind turbine J;
   [4 5 3 7| 6 9 10| 1 2 8] → [4 5 7 6| 9 3 10| 1 2 8]
5. Modify locations of string breaks.
   [4 5 3 7| 6 9 10| 1 2 8] → [4 5 3| 7 6 9| 10 1 2 8]

Operators 6 to 8 represent a combination of the first five cases and are therefore not shown in this example.

These new solutions are then placed back as set in the population in the fifth step. This process iterates until a set precondition is met. Possible preconditions are a certain maximum amount of computational time, a number of iterations or no significant improvement in the total solution. For this purpose, iterations are stopped when no significant

improvement of the total solution (order of 0.01%) in the latest 100 iterations is found. Eventually, the best solution in terms of total weight is chosen as the near optimal.

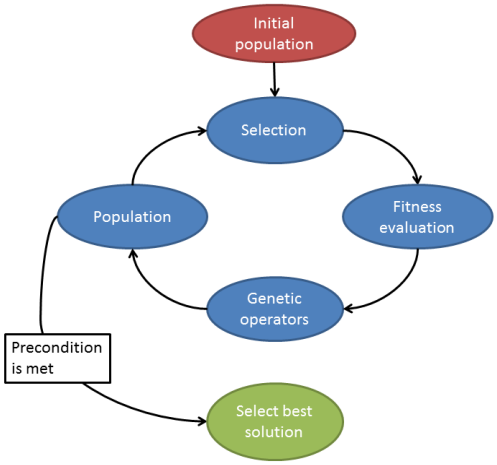

Figure 5: Genetic algorithm used in the optimization under a flat seabed (Roetert, 2014).

2.2 Optimization under a dynamic seabed

After the optimization under a flat seabed, all connections between two turbines are optimized under a dynamic seabed. As opposed to the cable layout determination, now morphological development of the seabed is taken into account. This development is present in the form of bedform growth and decay as well as bedform migration. In this step only the already determined connections between the turbines are optimized, while turbine connectivity remains fixed.

In order to properly analyse effects of the method, the connections are optimized separately in the vertical (into the bed) and horizontal (pathways between the turbines) plane. Results are addressed in total costs per connection. Aim for this method is to minimize risks and costs for each connection. This section describes subsequently the morphological evolution of the seabed, the cost function, the algorithm used for the vertical bed optimization and Dijkstra's algorithm used in the horizontal optimization.

2.2.1 Morphological evolution of the seabed

As discussed in Section 1.1, sand wave migration poses a great threat to cable failure. In sand wave fields, depending on the location of cable sections underneath the sand waves, the net bed level change over the design life of the wind farm will typically be either positive (bed level rise) or negative (bed level drop).

Cable sections on or near the crest of a sand wave will typically experience a net receding seabed over the design life of the wind farm. Alternatively, cable sections near a sand wave trough will most typically experience a rising seabed throughout the duration of their design life. Cable sections initially constructed on the lee side of a crest or the stoss side of a trough point however, may experience both rising and falling bed levels. The net seabed level change at such sites will typically be much lower than those buried directly under a crest or trough point. These possible modes of seabed level change are summarized in Figure 6. However it must be stressed that if sand waves do not migrate very fast, e.g. a quarter wavelength over the cable design lifetime, the maximum seabed drop and rise occur at the steeper parts of the stoss and lee side.

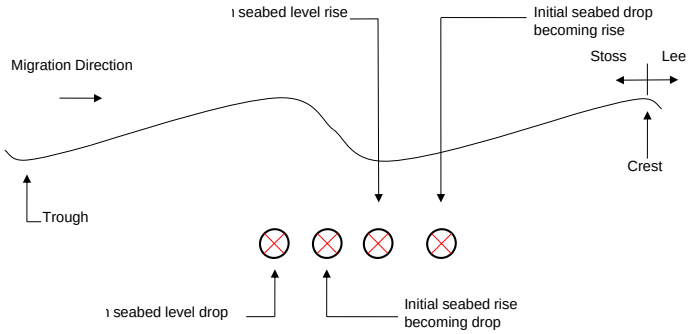

Figure 6: Schematization of general sand wave dynamics above a buried cable relative to its horizontal position.

In order to quantify the morphological evolution of the seabed over the lifetime of a wind farm, the minimum seabed level observed within this period has to be determined. Figure 7 shows an example of the development of the sand wave elevation within the period 2002-2017 for a certain point in a sand wave area. It can be observed that the lowest bed level occurred in 2012, whereas the present seabed already lies 2 m higher in the water column.

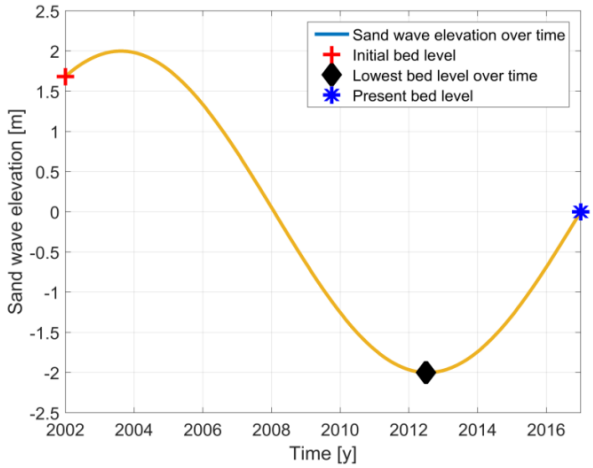

Figure 7: Sand wave elevation relative to the surrounding seabed over time.

Deltares (2016) presents an extensively overview of state-of-the-art techniques used to determine the minimum seabed level over a certain time period, applied to the Dutch wind farm area "Hollandse Kust (zuid)". In this area where seabed dynamics is mainly limited to sand wave migration, the following steps are applied:

Data collection:

1. Collection of available bathymetrical data (preferably covering a period of 20 years), hydrodynamic data and geological data.

Morphodynamic characterization of the wind farm area:

2. Separation via filtering of the static (e.g. sand banks) and the mobile components of the seabed (e.g. sand waves and megaripples). For this purpose a coarse spatial filtering of the bathymetry was applied on the three available surveys. The filter size was chosen such that the mobile bedforms (i.e. sand waves and megaripples) could be removed, while the underlying bathymetry remains unaltered in shape and is not noticeably smoothened by the filtering process. The filtering was carried out with a mean filter with

a compact base of 1400 m and results in the static part of the seabed. The dynamic part is obtained by subtracting the static bathymetry from the actual bathymetry.

3. Assessment of the dynamics of the static part of the seabed via the change in bed level over time ($\delta z / \delta t$ method) to verify that the static part can indeed be considered static over the lifetime of the wind farm.
4. Analysis of the geological composition of the substrate in the area with a special focus on the potential presence of non-erodible layers. This step is to investigate whether future seabed level variations may be affected by the local geology.
5. Numerical modelling of tidal flow and net-sediment transport to obtain an estimate of the spatial variation of sand wave dimensions and their directions and migration rates over the wind farm area. The model results are used as a verification of the directions determined in step 6.

Morphodynamic analysis for rhythmic bedforms:

6. Automated detection of sand wave migration directions. Migrating sand waves are in general characterized by a mild sloping stoss side and a steeper lee side oriented in the direction of propagation. Furthermore, sand waves tend to migrate in a direction roughly perpendicular to the crest in the direction of the steepest gradient, which in Deltares (2016) was found to correlate well to the direction of the net sediment transport (step 5). For this step the dynamic part of the seabed (step 2) is used. By differentiating the filtered dynamic part of the bathymetry, the direction of the sand wave crest can be estimated. This is illustrated in Figure 8, where the direction of the gradient field is shown in the top plot, whereas the magnitude of the gradient along a transect is shown in the bottom plot.

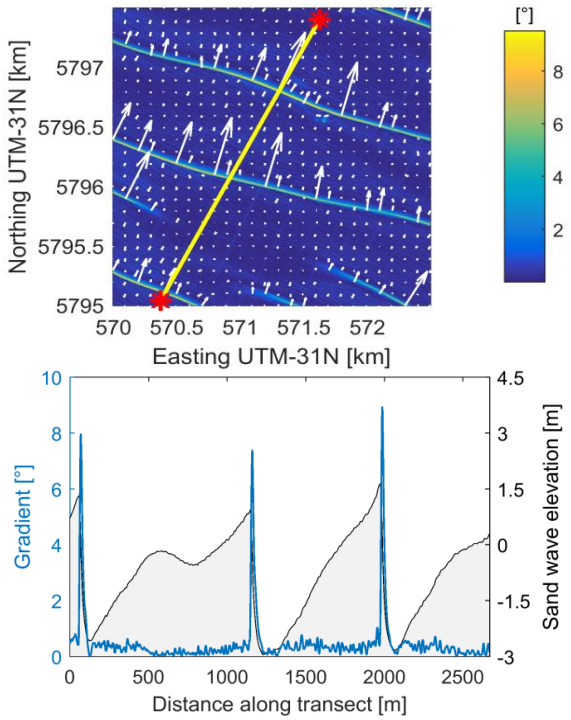

Figure 8: Top: Gradient of the Sand Wave Field. Colours and arrows indicate the direction of the point wise gradient. Please note that the number of arrows is down sampled for illustration purposes. Bottom: Spatial gradient in degrees from the horizontal plane along the transect indicated in the top plot (Deltares, 2016).

7. Optimized cross-correlation technique for automated analysis of several thousands of transects covering the wind farm area. For each transect, information is extracted from the filtered sand wave fields of two independent bathymetries and the spatial offset is computed using a 1D cross-correlation. The cross-correlation determines the migration distance which will give the minimized error between the two bathymetrical transects as illustrated in Figure 9.

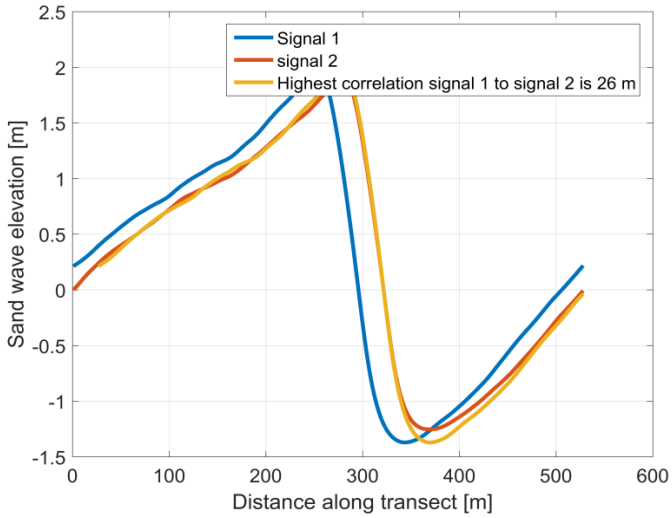

Figure 9: Example of cross correlation analysis as carried out for individual sand waves (Deltares, 2016).

8. Estimating uncertainty range based on measurement errors, processing inaccuracies and smaller scale seabed features such as megaripples. Megaripples are included in the uncertainty band, as the megaripples present on top of the sand waves have, due to their irregular pattern and high migration speeds, a neglectable influence on power cable integrity (Figure 2).
9. Migration of sand wave fields with calculated migration rates and directions. In Deltares (2016) three migration directions (lower bound, best estimate and upper bound) and three migration speeds (minimum, mean and maximum) are used, resulting in nine predictions for each year in the predicted period (e.g. 2017 to 2051 in Deltares (2016)).
10. The lowest seabed level is estimated by the lower envelope of all predicted dynamic bathymetries combined with the downward uncertainty band and the static bathymetry. The difference between the present bathymetry and the lowest seabed level is the maximum seabed lowering over the considered period. Similarly, the highest seabed level during the lifetime of the wind farm is determined.

2.2.2 *Cost function*

To determine total cable costs, a cost function has been set up. This function contains cost elements involved in cable installation and calculates costs at a chosen moment in time corresponding with the latest available bathymetry. Costs of surveying the cable route are not taken into account. Broadly the function is divided in the following three parts:

- CAPEX – Capital expenditures, here initial cable costs (cable costs per meter, excavation costs per meter);
- OPEX – Operational expenditures, here monitoring costs (costs of cable reburial);

- Costs of cable failure – Costs of an event to happen (power loss) multiplied with the internal and external risks.

Since bed levels are not constant over a certain area, a connection between two turbines is divided in segments. The length and type of each section is different for the horizontal and vertical optimization. Based on the three parts, the cost function is defined as:

$$Costs(turbine\ x - turbine\ y) = CAPEX(C_i) + OPEX(C_i + Ch_{bed}) + (R_{int} + R_{ext}) * \left(Power\ loss + CAPEX(C_r)\right)$$

The function describes the costs for a connection between turbine x and y. C_i describes the initial coverage, Ch_{bed} change in bed level in a given period and C_r defines required burial depth for the new cable to be installed. The internal and external risks are defined by R_{int} and R_{ext} respectively. The power loss as a result of failure is calculated from revenues missed. Here turbine capacity, number of turbines affected (so a string failure next to the OHVS affects more turbines than a failure at the end of a string), turbine capacity factor (average percentage of maximum capacity produced), revenues per kWh and the average downtime are taken into account. Power loss is described by:

$$Power\ loss = Turbine\ capacity * number\ of\ turbines\ affected * capacity\ factor * revenues\ per\ kWh * average\ downtime$$

When a piece of cable becomes exposed on the seafloor, the flow around it can induce cable vibrations. This can lead to further un-burial and cable fatigue. However, as cable exposure is considered a worst case scenario, the risk of failure rises significantly when becoming exposed. Assigning a very high risk assures that possible exposure is prevented.

Internal risks can be seen as probability of failure caused by faults in the cable multiplied with the costs of failure (power loss times the new cable CAPEX). Faults can originate from the cable manufacturing, cable laying/ trenching, covering process and overheating. Only the risk of overheating changes for different burial depths. The internal risk is defined based on expert input and Holmstrøm (2007) and can be described by:

$$Risk(internal)\ [y^{-1}] = (0.015 + 0.030 \cdot (C_i + Ch_{bed})) * \left(Power\ loss + CAPEX(C_r)\right)$$

External risks can be seen as human induced hazards endangering the power cable from the outside. The hazards are always associated with a physical impact in the form of penetration or drag. In Appendix A of DNV's 'Recommended Practice DNV-RP-J301, "Subsea Power Cables in Shallow Water Renewable Energy Applications", February 2014' (DNV, 2014) a summary of hazards is presented. The hazard overview in DNV-RP-J301 has been used as a guidance and checklist to develop a first global external risk assessment for the infield and export cables. All relevant external risks are quantified according to Appendix C in (Roetert, 2014).

An external risk is quantified as the probability of an failure event to happen calculated by multiplying the product of the return period and the probability of actual damage by the costs of failure (power loss times the new cable CAPEX). Identified external risks are valid up to a certain depth below the seabed, an anchor for example protrudes the seabed much less than for example stranded ships. Also the risk of failure decreases when going deeper into the seabed. The subjective probabilities of cable damage are indicated for a 1m burial depth. As a guidance it is suggested that for each 50% reduction or increase of burial depth the probability of damage caused by an event respectively increases or decreases by one order of magnitude. To illustrate possible external risks and their probability of cable damage, Table 1 and Table 2 provide four examples for both penetrating and dragged objects.

Table 1 Examples of external risk caused by penetrating objects with their estimated probabilities

Likely type of event	Estimated penetration in seabed	Estimated risk of damage cable/year
Spudcan positioning error	1,0 – 2.0 m	10^{-8}
Anchor drop	<0.5 m	10^{-8}
Dropped materials during maintenance	0.5 – 2.0 m	10^{-3}
Lost freight from vessels/boats	0.5 – 1.0 m	10^{-7}

Table 2: Examples of external risk caused by dragged objects with their estimated probabilities

Likely type of event	Estimated penetration in seabed	Estimated risk of damage cable/year
Anchor drag during mooring	2.0 m (drag <20 m)	10^{-6}
Anchor chain drag during emergency mooring	0.25 m	10^{-6}
Fishing net drag	0.25 m	10^{-4}
Trencher deviates from planned route	0.5 – 2.5 m	10^{-3}

2.2.3 Vertical bed optimization algorithm

The basis for the vertical bed optimization is formed by an optimization algorithm designed for this purpose. Goal of the algorithm is to determine the optimal initial burial depth along a connection between two turbines. The optimization algorithm used is an extension of the cost function, tailored to finding the optimal initial burial depth. To calculate the optimal burial depth the following steps are taken, the letters between brackets refer to the algorithm presented below:

1. Divide the connection between two turbines *(i)* in a number of segments with equal length *(s)*. The length of each segment needs to be sufficiently small in comparison with the sand wave length, in order to avoid significant differences in bed level lowering between two adjacent segments. It is advised to use segment lengths in the order of 1 m.
2. Vary for each section the initial burial depth between 0 m, being exposed to the seabed, towards the maximum possible initial burial depth *(Burial)*. Intermediate steps are chosen as small as possible (in the order of 0.01 m), to prevent sharp transitions between segments. In addition the risk of failure per segment is determined by dividing risk of failure for that particular segment by the number of segments present.
3. Determine for each section the optimal initial burial depth in terms of minimized costs *(C(I,s))* and combine all segments. Total costs and risks per connection *(TotalC(i)/TotalR(i))* are calculated by adding up the costs and risks for all segments. Sharp transitions between segments are avoided as segments lengths are sufficiently small compared to differences in the predicted bed level lowering of sand waves, which spread out over tens of meters.

The added steps combined with the cost function, lead to the following optimization algorithm:

$for\ i = 1{:}\ noConnections$
$for\ s\ =\ 1{:}\ noSegments$
$for\ Burial = 0{:}\ \max \text{Burial}\,(cm)$
$Costs(Burial) = (CAPEX(C_i(s, Burial)) + OPEX(C_i + Ch_{bed}(s, Burial)) +$
$(R_{int}(s, Burial) + R_{ext}(s, Burial))\ /\ noSegments * *$
$(Power\ loss\ + CAPEX(C_r(s, Burial)))$
end

$OptBurial = 0 + (find\ (\min\ (Costs)) - 1)/100$
$C(i, s) = \min(Costs)$
$R(i, s)$
$= (Rint(s, -OptBurial) + Rext(s, -OptBurial))/noSegm\,IBurial(i, s)$
$IBurial(i, s) = 0 +\ OptBurial$
$= 0 +\ OptBurial$
end

$TotalC(i) = sum(C(i, :))$
$TotalR(i) = sum(R(i, :))$
end

2.2.4 Dijkstra's algorithm

Underlying the horizontal optimization is Dijkstra's algorithm. The algorithm is first described by Dijkstra (1959) and searches for the shortest path between two given vertices for a graph with weighted edges (length of each connection) and empty vertices (i.e. vertices that are not contributing to the route weight). The algorithm uses two distinct arrays to record the structure of the shortest path in the graph G (Pemmaraju & Skiena, 2003). A similar algorithm is used in Pillai et al. (2015), using Dijkstra's algorithm for routing around constraints:

1. The distance array: For point i on the graph, dist (i) maintains the length of the shortest path known between the starting point s and i. For example dist (*s*) should be zero as the route is still at is starting point. The distances towards each point not included in the route are denoted as dist *(i)* = ∞
2. The parent array: For each point *i* on the graph, parent (*i*) maintains the predecessor of i on the shortest path from *s* to *i*.

Dijkstra's algorithm goes through *n-1* iterations. *n* stands for the number of points on the graph, as the distance to the starting point is zero; there is no shortest path to the first point. The efficiency of the algorithm depends on the following observation:

S is the set of points for which the shortest path is already found. So the distance array includes the correct distance towards all points *i* ∈*S*. Then, among all points not in *S*, point *i* with the smallest distance towards *S* has its distance value set correctly (Dijkstra, 1959). During each iteration, the points not in S are scanned for point i with the smallest distance. From this point, all routes (i,j) to other points are analysed and adjusted if the distance to point i plus the weight (i,j) is smaller than the shortest path to point j.

When the distance array contains the shortest distances from point s to every other point on the graph, it can be said that for any edge *(i,j)* with weight *w(i,j)*, dist $(j) \leq dist\ (i) + w(i, j)$. This statement says that for all routes (i,j) with a specific weight, the distance to point j is smaller than or equal to the distance to point i plus the route weight. When the inequality in the statement holds, another route towards point j is shorter. The routes *(i,j)* for which the inequality holds are denoted as relaxed. At the termination of the algorithm, all routes are relaxed and the distance array contains the correct shortest-path distances. Figure 10 depicts an example of Dijkstra's algorithm applied on a graph, showing edge weights and shortest routes towards each vertex. The shortest path in terms of total weight is denoted via the dotted edges and grey vertices.

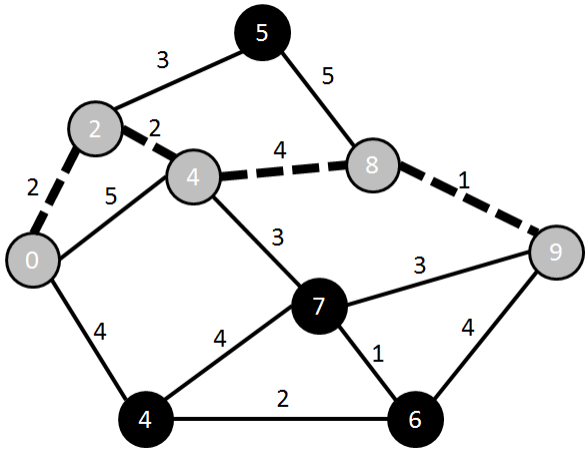

Figure 10: Example of Dijkstra's algorithm with edge weights, shortest distance towards each vertex and the optimized shortest route (dashed edges and grey vertices).

3 APPLICATION OF THE OPTIMIZATION ALGORITHMS

In this section, the steps taken to apply the optimization algorithms and to calculate the cable route layout are described. The flow chart of all steps is depicted in Figure 11.

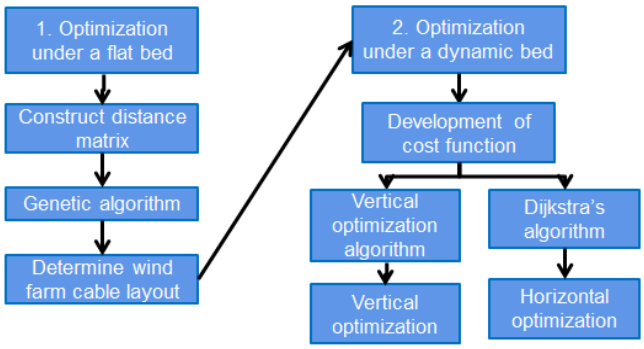

Figure 11: Flow chart depicting the flat and dynamic bed optimization steps, optimization, together with the underlying functions and algorithms.

3.1 Flat bed optimization

First optimization step is to find the layout with minimal total costs under a flat seabed. For this optimization step the weight of the edges is set equal to the distance between the turbines with a possible added weight due to constraints along the connection. To calculate the optimal wind farm cable layout assuming a flat seabed the following steps are performed:

1. Determine the locations of wind turbines and the OHVS.
2. Set optimization constraint, such as maximum string capacity and requirement that cables should not cross.
3. Assign weights to all edges, here distance between two considered turbines with possible added constraint weights.
4. Apply the genetic algorithm to the wind farm and determine the most optimal layout in terms of total length.

3.2 Vertical optimization

First part of the dynamic seabed optimization is to find the most optimal position in the vertical plane such that cable burial is guaranteed and risks and costs are minimized. This means that areas which are subject to large seabed lowering require a larger initial burial depth.

To calculate the optimal burial depth in the vertical plane for a certain connection between two turbines, the following steps are performed:

1. Calculate the seabed lowering between two turbines by subtracting the present bathymetry from the calculated lowest seabed level.
2. Work out the vertical optimization algorithm (Section 2.2.3) with aid of the cost function (Section 2.2.2).
3. Calculate costs, risks and savings per connection.

It must be stressed that the added cable length as a result of varying initial burial depths is negligible compared to the total cable length.

3.3 Horizontal optimization

Next to the vertical optimization, ideal cable positions in the horizontal plane are investigated. With aid of this method, cables can be routed around subsiding areas, reducing risks and total costs. To determine the optimal cable path in the horizontal plane, the following steps are performed:

1. Create a grid around a connection between two turbines and calculate the seabed lowering by subtracting the present bathymetry from the calculated lowest seabed level. A sufficiently small grid size (here: 1x1 m) is required in order to avoid sharp transitions in bed level lowering between the grid points. For sand waves significant differences in bed level lowering are present on a horizontal scale of tens of meters.
2. Apply cost function to the edges connecting the grid points, assuming a constant initial burial depth (Section 2.2.2). Note that only connections to adjacent cells are considered.
3. Determine the cheapest path through the grid by means of Dijkstra's algorithm (Section 2.2.4) and determine cost and risk savings.

4 RESULTS

In this section the effects of cable route optimization are discussed by means of a case study. First a description of the case study is given, followed by results of the flat and dynamic bed optimization.

4.1 Case study

In order to assess the applicability of the cable route optimization, a wind farm case study is performed. Requirements for the wind farm case study are: availability of sufficient bathymetrical data, dynamic seabed environment, geological data of the subsoil and hydrodynamic data of the area.

Deltares (2016) extensively studied the Hollandse Kust (zuid) Wind Farm Zone (HKZWFZ), providing design seabed levels for the period 2016-2051. HKZWFZ is located off the Dutch coast and is sub-divided into four sites. The morphology in the wind farm zone is classified as dynamic with sand waves and megaripples covering the entire area.

For this case study, the focus will be on site I, as this site experiences highest sand wave migration speeds and largest seabed lowering. As depot, the HKZ Alpha platform is used. 45 turbine locations are defined randomly assumed 8MW turbines and a mutual distance of 1200 m. Figure 12 depicts the maximum seabed lowering in site I predicted for the period between 2016 and 2051 together with turbine and platform locations. Note that the maximum lowering could have occurred halfway through the prediction period.

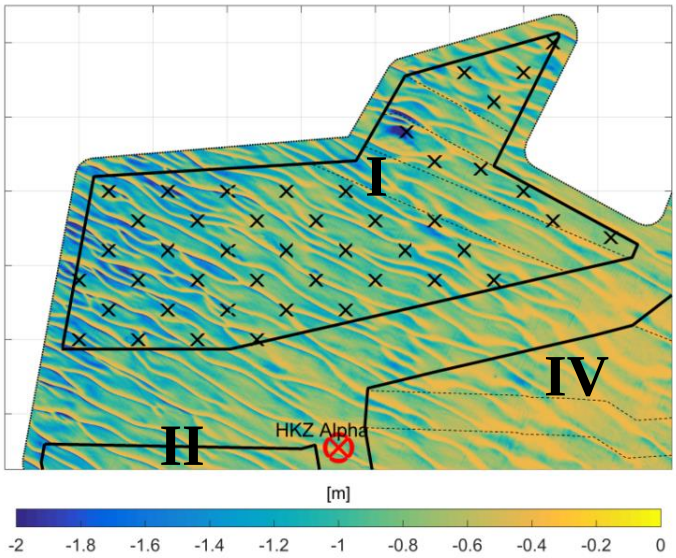

Figure 12: Maximum seabed lowering observed in site I of the HKZWFZ observed within the period 2016 - 2051. The black crosses denote fictitious turbine locations, while the HKZ Alpha platform is located to the south. Site IDs are identified with roman numbers.

4.2 Optimization under a flat seabed

The optimization is started with the assumption of a flat seabed at a certain point in time. Because of this flat seabed, edge weight is calculated as the distance between two turbines together with added weight related to possible constraints. For the HKZWFZ three cable constraining areas are designated: first cables should not go outside the site boundary (except for connections towards the OHVS) and crossings of the two cable corridors (red dotted areas in Figure 13) should be minimized. With aid of the genetic algorithm and the constraints of not crossing and a maximum number of turbines per string, a most optimal layout is calculated.

The layout found after 566 iterations assuming seven turbines per string is depicted in Figure 13. It is observed that cables never go outside the wind farm site and that the cable corridors are crossed only three times, which is the minimum amount of crossings given string capacity (seven) and the amount of turbines located behind the corridors (ten). Since string capacity depends on the type of cable used (33 kV or 66 kV) and the turbine capacity (e.g. 3 MW versus 8 MW), Table 3 provides the total route length for different string capacities.

Table 3: Total route length for a number of string capacities to connect 45 turbines.

String capacity	Number of strings	Total route length [m]
5	9	93659
6	8	88176
7	7	80836
8	6	77121
9	5	75157
10	5	73669
12	4	69448

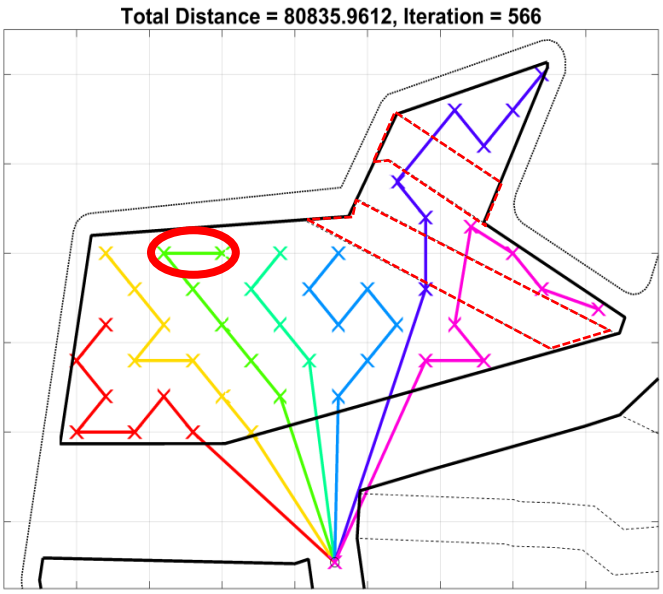

Figure 13: Wind farm layout found for random turbine locations in the HKZWFZ site I. The oval denotes the connection optimized in Section 4.3 and the two dotted areas denote the two cable constraints in HKZWFZ.

Results for different string capacities denote that more strings increase total route length; also cable constraints come in to play when changing string capacity. For example, with a minimum string capacity of ten turbines, only one crossing per corridor is required. String capacity however is bounded to several limitations. In addition, longer strings cause more power outage in case of cable failure next to the HKZ Alpha platform. It must be stressed that the total route lengths found in Table 3 are near optimal solutions and can only be regarded as most optimal when all solutions are analysed.

4.3 Optimization under a dynamic seabed

The layout found in Section 4.2, assuming a string capacity of seven turbines (depicted in Figure 13) is chosen for further optimization under a dynamic bed. This section is divided in four parts: Cost function parameters, optimization in the vertical plane, optimization in the horizontal plane and a sensitivity analysis. To illustrate both the vertical and horizontal optimization, a connection is chosen which is strongly influenced by sand wave migration. The chosen connection is denoted by an oval in Figure 13 and in Figure 14 as a zoom in plot of Figure 12.

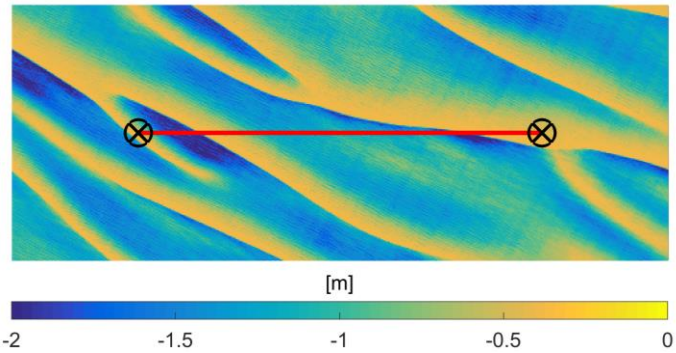

Figure 14: Detailed seabed lowering predicted for the connection used to illustrate in the vertical and horizontal optimization.

4.3.1 Cost function parameters

To conduct optimization under a dynamic bed the input for the cost function and the risk parameters need to be quantified. Parameter values are determined based on literature, expert judgement and comparable cases as determined in Roetert (2014). Note that a fixed value is chosen for the excavation costs; preferably this should vary with burial depth. Table 4 gives an overview of the cost function parameters valid at the start of the study, their corresponding values and their source.

Table 4: Values for cost function parameters valid at the start of the study (Roetert, 2014).

Parameter	Value	Source
Capital expenditures		
Cable material costs per meter	€300	Expert judgement
Cable trenching costs per meter	€400	Expert judgement
Repair costs	€2.000.000 - €3.000.000	Expert judgement
Powerloss		
Average downtime	2-6 months	Expert judgement
Turbine capacity	8.0 MW	Turbine developments
Capacity factor	0.41	(Andrew, 2014; EWEA, 2014)
Revenues per kWh	€0.15	Expert judgement

4.3.2 Optimization in the vertical plane

The dynamic bed optimization is started with finding an optimal position in the vertical plane, with a fixed position in the horizontal plane, e.g. a straight line between two turbines. For the chosen connection (Figure 14), the vertical optimized cable position is depicted in Figure 15. Clearly visible is the seabed lowering (difference between blue and black line in top plot) due to sand wave migration and the added uncertainty band.

When not taking seabed morphodynamics into account, it is assumed that power cables are buried with a constant burial depth of 1.5 m (dashed red line). Indicated by red arrows in Figure 15 it is observed that the power cable can become exposed on the seabed and can become prone to cable failure. Optimizing the initial burial depth (green line in the bottom plot) assures that minimum cable coverage (straight blue line in the bottom plot) is guaranteed over the wind farm life time. This minimum cable coverage is calculated by applying the cost function onto the chosen connection. Note that the initial burial depth is smoothened to fulfil maximum cable bending restrictions.

It can be argued that the complex initial burial depth influences cable installation efficiency negatively, i.e. constant adjustments and checks have to be made to see if the excavation equipment reaches the correct depth. Sand wave dynamics can however lead to significant differences in bed level changes over a cable transect. In HKZWFZ, where seabed dynamics are a result of sand wave migration, these differences can range up to 4 m within certain cable strings. When assuming a fixed initial burial depth (e.g. the average of the optimized initial burial depth depicted in Figure 15), cable segments experiencing a relatively small seabed lowering (order of 0 to 1 m) or seabed rise, are always subject to a large burial depth, resulting in higher risks of overheating and high cable installation costs. In contrary, cable segments subject to a large seabed lowering (more than 3 m) have an increased risk of failure due to limited burial depth or even exposure. By introducing a varying initial burial depth, risks are minimized per segment instead of averaged over the total cable length. Also cable burial can be performed faster in segments where smaller burial depths need to be achieved.

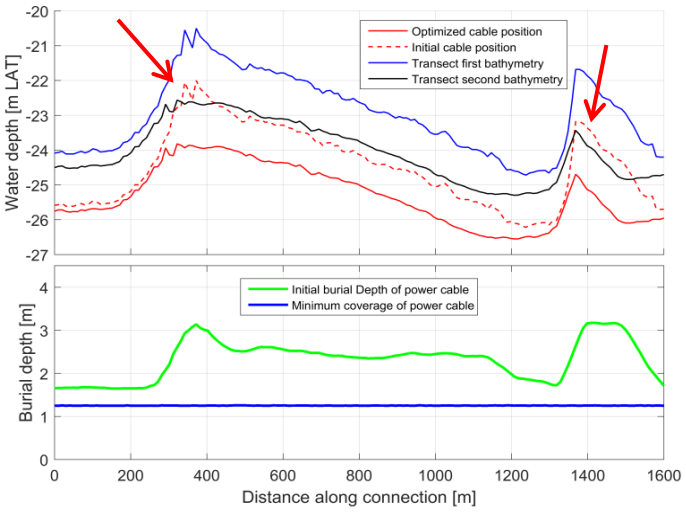

Figure 15: Optimized cable position in the vertical plane between two turbines. The top plot depicts the present bathymetry (blue line), lowest seabed level over time including uncertainty (black line), the initial cable position assuming a constant burial depth (dashed red line) and the optimized cable position (red line). The bottom plot depicts the optimized initial burial depth (green line) and the minimum cable coverage over the period considered (fixed blue line). The red arrows indicate locations where the cable can become exposed, when buried at a constant burial depth of 1.5 m.

With aid of the cost parameters defined in Table 4 and the quantified risks, cost savings and risk reduction are calculated by comparing costs and risks for a cable with a fixed burial depth of 1.5 m to the optimized initial burial depth. For optimized cable position depicted in Figure 15 cost savings (CAPEX plus failure costs) of 46 % and a risk reduction (probability of failure times the costs of failure) of 76 % are achieved. However, it must be stressed that in cases a cable becomes exposed on the seabed, the risk of cable failure increases drastically. Overall a cost reduction of 71 % is achieved. This number is highly influenced by the reduced power loss due to cable failure close to the platform, i.e. when a string next to the platform fails, all turbines in the specific string cannot transfer power to the platform.

4.3.3 Optimization in the horizontal plane

The second part in the dynamic bed optimization is to find the most optimal route in the horizontal with aid of Dijkstra's shortest route algorithm and the cost function assuming a constant initial burial depth.

When not taken seabed dynamics into account the cable route is assumed to follow a straight line between the two turbines considered. For the chosen connection (Figure 14), the horizontally optimized cable position is depicted in Figure 16. Clearly visible is the cable routing around a high cost area. By comparing the costs in Figure 16 with the seabed lowering in Figure 14, it is concluded that the high costs areas (yellow areas) are located in places where seabed lowering is most severe. As discussed in Section 2.2.1 these areas correspond to the sand wave crests. The cheaper parts (dark blue) are located in the sand wave troughs. Since the troughs are already at the lowest seabed level, predicted seabed lowering is equal to the uncertainty band.

With aid of the cost parameters defined in Table 4 and the quantified risks, a cost saving of 30 % and a risk reduction of 65 % is achieved for the considered connection compared to a straight connection between the two turbines. Overall a cost reduction of 30 % is achieved. This number is slightly lower than the vertical optimization outcome and is mainly influenced by the additional cable length.

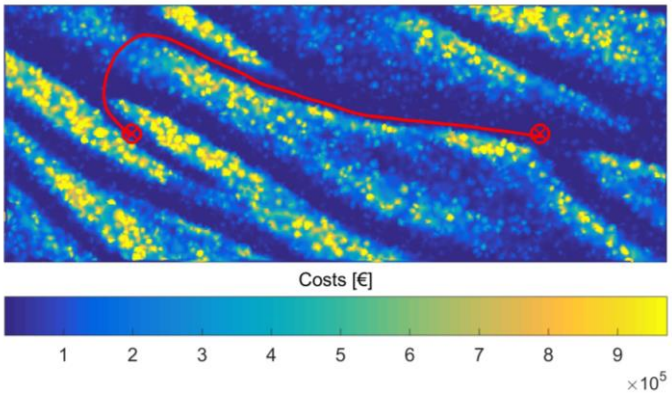

Figure 16: Optimized cable position in the horizontal plane between two turbines. The red line indicates the most optimal route calculated with aid of both the cost function and Dijkstra's algorithm. The grid displayed is calculated by applying the cost function on all edges. Yellow locations indicate areas with significant seabed lowering and higher costs, whereas the dark blue areas represent the cheaper areas subject to little seabed lowering.

4.3.4 Cost function parameter sensitivity analysis

Figure 15 and Figure 16 indicate that the cost function searches for an optimal minimum cable coverage. For the HKZ case study, based on parameter values presented in Table 4, a value of around 1.2 m was found. In order to assess the sensitivity of the cost function to changing parameter value, a sensitivity analysis is performed by varying some parameters separately with a 50 percent decrease and increase.

The cost function parameter sensitivity for the HKZ case study is shown in Table 5, describing the effect on total costs for the connection assessed in Section 4.3.2 and 4.3.3. Both the result on the route costs after vertical and horizontal optimization are calculated. To illustrate the results, Figure 17 depict the relative influence of cost function parameter on cable costs. Percentages are calculated via the cost function assuming the connection assessed in Section 4.3.2 and 4.3.3 after optimization in the vertical plane. When assuming a not optimized connection, the relative influence of expected costs of both repair and power loss at the expense of relative influence of cable material costs and excavation costs.

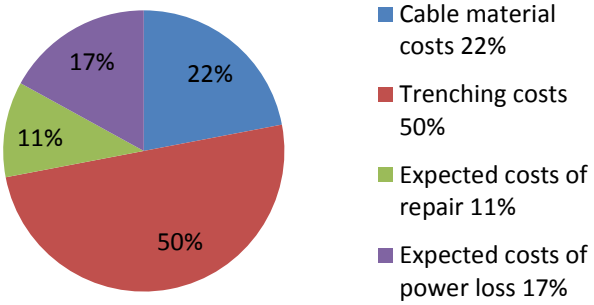

Figure 17: Relative influence on cable cost based on the connection assessed in Section 4.3.2 and 4.3.3 assuming optimization in the vertical plane. Note that expected costs of repair and expected power loss are multiplied by probability of cable failure.

Outcomes of the sensitivity analysis indicate that total route costs are mainly influenced by parameter magnitude, meaning that a 50% change in the larger parameter values (e.g. excavation costs) are more influencing results than a 50% change in the smaller parameter values (e.g. revenues per kWh). Sensitivity for both the vertical and horizontal optimization is comparable.

Table 5: Cost function parameter sensitivity for a connection in HKZWFZ. Percentage changes presented depict the difference between the base case presented in Section 4.3.2 and 4.3.3 and the costs assuming a 50 percent decrease or increase in parameter value.

Parameter	Case	Vertical optimization	Horizontal optimization
Cable material costs	+/- 50 %	+/- 11.4 %	+/- 15.6 %
Cable trenching costs	+/- 50 %	+/- 25.7 %	+/- 18.7 %
Revenues per kWh	+/- 50 %	+/- 9.4 %	+/- 8.7 %
Costs of repair	+/- 50 %	+/- 3.5 %	+/- 2.9 %
Probability of failure	+/- 50 %	+/- 12.9 %	+/- 11.6 %

5 CONCLUSIONS & DISCUSSION

This research shows that cable route optimization yields a significant contribution in reduction of costs for offshore wind farm construction and maintenance. The newly introduced dynamic bed method showed cost and risk reductions for all connections optimized in the vertical and horizontal plane.

The dynamic bed method presented in this research is a combination of methods presented in literature together with improved approaches of predicting dynamic changes to the seabed. Results are therefore inherent to uncertainties. Especially the newly setup cost function contains a large number of uncertainties. During the research, parameter values were assumed fixed based on expert judgment. In order to determine sensitivity of the results, a quick parameter sensitivity analysis was conducted, by increasing and decreasing parameter values separately with 50 percent. The analysis indicated that total cabling costs are mainly influenced by parameter magnitude, i.e. larger parameter values also give the biggest changes in costs. From Figure 17 it can be observed that the biggest part of cable costs for the specific optimized cable connection is covered by cable installation. Therefore, a 50 % change in this parameter has the largest relative influence on the total costs.

Furthermore, during the horizontal optimization, the initial cable burial depth is constant for all connections. It is assumed that including the vertical optimization mitigates the risk of cable failure and even more cost and risk reduction can be achieved. In this research, combining the horizontal and vertical optimization was not deemed possible due to a needed adjustment to the cost function.

The aim of the research was to construct tools to optimize cable routings applicable on a variety of offshore wind farms. Up to now the cable routing is assessed for the existing Prinses Amaliawindpark in (Roetert, 2014) and the planned Hollandse Kust (zuid) offshore wind farm presented in this research. As both wind farms are subject to a variety of dynamic seabed features, it is assumed that the route optimization tools are applicable to other case studies in morphodynamic environments with predictable sand wave migration.

ACKNOWLEDGEMENTS

This research was supported by the FLOW research program as part of the research project '*Optimizing cable installation and operation, a life cycle perspective'*, STW-project EUROS *(P14-03, 'Excellence in Uncertainty Reduction of Offshore wind Systems')* and the strategic research program '*Coastal and Offshore Engineering´* of Deltares, co-funded by the Dutch Ministry of Economic Affairs. Furthermore, we would like to acknowledge the Netherlands Enterprise Agency for allowing the use of the data and study results regarding the morphodynamics in Hollandse Kust (zuid).

REFERENCES

Andrew. (2014). Capacity factors at Danish offshore wind farms. Retrieved October 14, 2014, from http://energynumbers.info/capacity-factors-at-danish-offshore-wind-farms

Bauer, J., & Lysgaard, J. (2015). The offshore wind farm array cable layout problem: a planar open vehicle routing problem. *Journal of the Operational Research Society, 66*(3), 360-368.

Besio, G., Blondeaux, P., Brocchini, M., & Vittori, G. (2004). On the modelling of sand wave migration. *Journal of Geophysical Research, 109*(4), 1-13.

Bijker, R., Wilkens, J., & Hulscher, S. J. M. H. (1998). *Sandwaves: Where and why.* Paper presented at the Proceedings ISOPE , vol. 2. International society of Offshore and Polar Engineering, Golden, CO, pp. 153-158.

Bondy, J. A., & Murty, U. S. R. (1976). *Graph theory with applications*. New York; Amsterdam; Oxford: Elsevier Science Publishing Co., Inc.

Borsje, B. W., Roos, P. C., Kranenburg, W. M., & Hulscher, S. J. M. H. (2013). Modeling tidal sand wave formation in a numerical shallow water model: The role of tubulence formulation. *Continental Shelf Research, 60*, 17-27.

Caldeira, T. C. M. (2009). *Optimization of the Multi-Depot Vehicle Routing Problem: an Application to Logistics and Transport of Biomass for Electricity Production.* (Master thesis), Technical University of Lisbon.

Deltares. (2008). Sand wave dynamics Bligh Bank, H5239. Delft: Deltares.

Deltares. (2016). Morphodynamics of Hollandse Kust (zuid) Wind Farm Zone; Prediction of seabed level changes between 2016 and 2051. Ref: 1230851-000-HYE-0003; final report, dated 22 December 2016. Retrieved from: http://offshorewind.rvo.nl/file/view/47910422/report-morphodynamics-of-hollandse-kust-zuid-wind-farm-zone-deltares.

Dijkstra, E. W. (1959). A note on two problems in connexion with graphs. *Numerische mathematik, 1*(1), 269-271.

DNV. (2014). Recommended practice DNV-RP-J301 Subsea power cables in shallow water renewable energy applications. Oslo: Det Norske Veritas AS.

EWEA. (2014). Wind energy statistics and targets. Retrieved October 14, 2014, from http://www.ewea.org/uploads/pics/EWEA_Wind_energy_factsheet.png

Holmstrøm, O. (2007). Survey of reliability of large offshore wind farms.

Huntley, D. A., Huthance, J. M., Collins, B., Liu, C.-L., Nicholls, R. J., & Hewitson, C. (1993). Hydrodynamics and sediment dynamics of North Sea sand waves and sand banks. *Philosophical Transactions: Physical Sciences and Engineering, 343*(1669), 461-474.

Jenkins, A. M., Scutariu, M., & Smith, K. S. (2013). *Offshore wind farm inter-array cable layout.* Paper presented at the PowerTech (POWERTECH), 2013 IEEE Grenoble.

Kumar, S. M., & Panneerselvam, R. (2012). A Survey on the Vehicle Routing Problem and its Variants. *Intelligent Information Management, 4*(3), 66-74.

Maurer, R. (2016). Power under the sea. Retrieved from: http://www.agcs.allianz.com/insights/expert-risk-articles/power-under-the-sea/.

Morelissen, R., Hulscher, S. J. H. M., Knaapen, M. A. F., Németh, A. A., & Bijker, R. (2003). Mathematical modelling of sand wave migration and the interaction with pipelines. *Coastal Engineering, 48*(3), 197-209.

Németh, A. A. (2003). *Modelling offshore sand waves.* (Doctoral dissertation), University of Twente.

Németh, A. A., Hulscher, S. J. M. H., & de Vriend, H. J. (2002). Modelling sand wave migration in shallow shelf seas. *Continental Shelf Research, 22*(18), 2795-2806.

Netherlands Enterprise Agency. (2015). Offshore wind energy in the Netherlands ; the roadmap from 1,000 to 4,500 MW offshore wind capacity.

Pemmaraju, S., & Skiena, S. (2003). *Computational Discrete Mathematics: Combinatorics and Graph Theory with Mathematica*. New York: Cambridge University Press

Pillai, A., Chick, J., Johanning, L., Khorasanchi, M., & de Laleu, V. (2015). Offshore wind farm electrical cable layout optimization. *Engineering Optimization, 47*(12), 1689-1708.

Roetert, T. J. (2014). *Optimization of offshore wind farm power cable routing: development of a tool that optimizes the power cable route design for offshore wind farms.* (Master thesis), University of Twente.